Optoelectronic transport properties in amorphous/crystalline silicon solar cell heterojunctions measured by frequency-domain photocarrier radiometry: Multi-parameter measurement reliability and precision studies

Y. Zhang,[1,2] A. Melnikov,[1] A. Mandelis,[1,3,a)] B. Halliop,[3] N. P. Kherani,[3] and R. Zhu[2]
[1]*Center for Advanced Diffusion-Wave Technologies (CADIFT), Department of Mechanical and Industrial Engineering, University of Toronto, Toronto, Ontario M5S 3G8, Canada*
[2]*Institute of Electronic Engineering and Optoelectronic Technology, Nanjing University of Science and Technology, Nanjing, Jiangsu 210094, China*
[3]*Department of Electrical and Computer Engineering, University of Toronto, Toronto, Ontario M5S 3G4, Canada*

(Received 24 December 2014; accepted 16 February 2015; published online 5 March 2015)

A theoretical one-dimensional two-layer linear photocarrier radiometry (PCR) model including the presence of effective interface carrier traps was used to evaluate the transport parameters of p-type hydrogenated amorphous silicon (a-Si:H) and n-type crystalline silicon (c-Si) passivated by an intrinsic hydrogenated amorphous silicon (i-layer) nanolayer. Several crystalline Si heterojunction structures were examined to investigate the influence of the i-layer thickness and the doping concentration of the a-Si:H layer. The experimental data of a series of heterojunction structures with intrinsic thin layers were fitted to PCR theory to gain insight into the transport properties of these devices. The quantitative multi-parameter results were studied with regard to measurement reliability (uniqueness) and precision using two independent computational best-fit programs. The considerable influence on the transport properties of the entire structure of two key parameters that can limit the performance of amorphous thin film solar cells, namely, the doping concentration of the a-Si:H layer and the i-layer thickness was demonstrated. It was shown that PCR can be applied to the non-destructive characterization of a-Si:H/c-Si heterojunction solar cells yielding reliable measurements of the key parameters. © *2015 AIP Publishing LLC.* [http://dx.doi.org/10.1063/1.4913659]

I. INTRODUCTION

Solar cells based on a-Si:H/c-Si heterojunctions have gained much attention recently due to their high efficiency as demonstrated by the so-called "Heterojunction with Intrinsic Thin layer (HIT)" solar cell technology which can achieve a solar conversion efficiency of 24.7%.[1] More recently, the application of these heterojunctions in interdigitated back contact cells has set a new world record of 25.6% photovoltaic conversion efficiency for silicon solar cells.[2] The structure of HIT cells is sketched in Fig. 1. It consists of a crystalline silicon (c-Si) wafer with thin layers of doped hydrogenated amorphous silicon (a-Si:H) and an intrinsic amorphous silicon layer (i-a-Si or i-layer) to form the junctions (the transparent conducting oxide layer and metal grids are not shown).

In amorphous thin film p-i-n solar cells, excessively high doping of the a-Si:H layers can lead to a reduction of the open-circuit voltage, due to increased defect concentrations in the layers.[3,4] Furthermore, a thick i-a-Si degrades the drift electric field necessary to enable carrier transport. Therefore, the doping concentration of a-Si:H and the thickness of i-a-Si are two fundamental factors which can limit the performance of amorphous thin-film solar cells.

Up to now, only few investigations have been published with a goal to optimize the doping concentration of the amorphous silicon layer and the thickness of i-a-Si.[5] In this paper, we use two groups of samples to investigate the influence of the doping concentration of the a-Si:H layer and the thickness of the i-layer on the transport parameters of the amorphous layer and the c-Si substrate, as these parameters determine and limit the efficiency of solar cells fabricated with this geometry. To evaluate the transport properties of the processed silicon wafers studied in this work, the PCR signal was measured as a function of the modulation frequency in the range from 10 Hz to 100 kHz. A 1-D two layer theoretical carrier density wave (CDW) and PCR model was applied to investigate the influence of the thickness of the i-layer and the doping concentration of the a-Si:H layer on the transport properties of the a-Si and c-Si layers, taking into account the effects of the unoccupied trap density at the nanolayer-substrate interface. In particular, the resulting measurements of the optoelectronic parameters of our samples, based on best multi-parameter fits of PCR theory to the data, were examined in terms of their reliability (implying uniqueness) and precision. These important issues arise in the commonly encountered situation of multi-parameter fits to frequency-domain modalities, such as PCR, which have only two signal channels (amplitude and phase).[6]

II. THEORY

The PCR signal is obtained by solving the carrier transport equation and integrating the carrier density diffusion

a)Author to whom correspondence should be addressed. Electronic mail: mandelis@mie.utoronto.ca

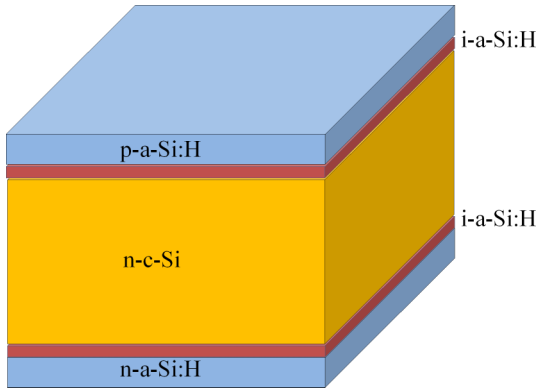

FIG. 1. Sketch of typical heterojunction silicon structures with n-type c-Si/p-type a-Si:H with an additional thin undoped i-a-Si:H layer.

wave over the thickness of the processed wafer. The one-dimensional cross-sectional geometry of a two-layer composite optoelectronic solid is shown in Fig. 2.

By taking into account the unoccupied trap density at the nanolayer-substrate interface, the boundary-value problem is described as follows:[7]

$$\frac{d^2}{dx^2}N_1(x,\omega) - \sigma_1^2 N_1(x,\omega) = -\frac{I_0(1-R)\beta_1}{2D_1}e^{-\beta_1 x}, \quad 0 \le x < L_1, \tag{1}$$

$$\frac{d^2}{dx^2}N_2(x,\omega) - \sigma_2^2 N_2(x,\omega) = -\frac{I_0(1-R)\beta_2}{2D_2}e^{-\beta_1 L_1 - \beta_2(x-L_1)}, \quad L_1 < x \le L_2, \tag{2}$$

$$D_1\frac{d}{dx}N_1(x,\omega)|_{x=0} = S_1 N_1(0,\omega), \tag{3}$$

$$N_1(L_1,\omega) - N_T(L_1) = N_2(L_1,\omega), \tag{4}$$

$$-D_1\frac{d}{dx}N_1(x,\omega)|_{x=L_2} + D_2\frac{d}{dx}N_2(x,\omega)|_{x=L_1} = S_i n_{Tf}, \tag{5}$$

$$-D_2\frac{d}{dx}N_2(x,\omega)|_{x=L_2} = S_2 N_2(L_2,\omega), \tag{6}$$

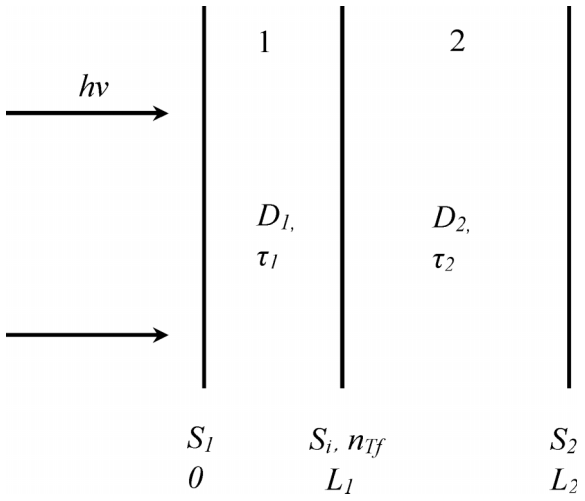

FIG. 2. Schematic representation of the cross-sectional geometry of a two-layer optoelectronic solid.

where

$$\sigma_j = \sqrt{\frac{1+i\omega\tau_j}{D_j\tau_j}};\ j = 1,2, \tag{7}$$

$$N_T(L_1) = n_{Tf}. \tag{8}$$

Finally, the PCR signal can be expressed as follows:

$$S_{PCR}(\omega) = C_{L_1}\int_0^{L_1} N_1(x,\omega)dx + C_{L_2}\int_{L_1}^{L_2} N_2(x,\omega)dx. \tag{9}$$

Here, N_1, D_1, τ_1, and β_1 are, respectively, excess CDW concentration, ambipolar diffusion coefficient, excess carrier lifetime, and absorption coefficient in layer 1. N_2, D_2, τ_2, and β_2 are the respective quantities in layer 2. S_1, S_i, and S_2 are front-surface, interface, and back-surface recombination velocities (SRVs). ω is the angular frequency of laser power modulation. I_0 is surface photon flux, R is surface reflectivity, and n_{Tf} is the number density of free (unoccupied) traps at the interface $x = L_1$.

To determine the transport properties of a processed semiconductor Si wafer like the one shown in Fig. 1, both the amplitude and the phase of the PCR signal were measured as a function of modulation frequency and then fitted to the foregoing theoretical model, Eq. (9). In view of the fact that several (7) unknown parameters had to be extracted from only two PCR signal channels (amplitude and phase), albeit over the entire frequency range (a substantial constraint), and in the absence of a rigorous mathematical proof of uniqueness of fit and measurement, in the multi-parameter fitting procedure we used two independent best-fitting computational programs to investigate the reliability and thus the uniqueness of the best-fitted results in a statistical analysis. The first program (labeled "mean-value best fit") minimizes the mean square variance between the experimental data and a linear combination of the theoretical values of both amplitude and phase, simultaneously. In the second program, we used the fminsearchbnd

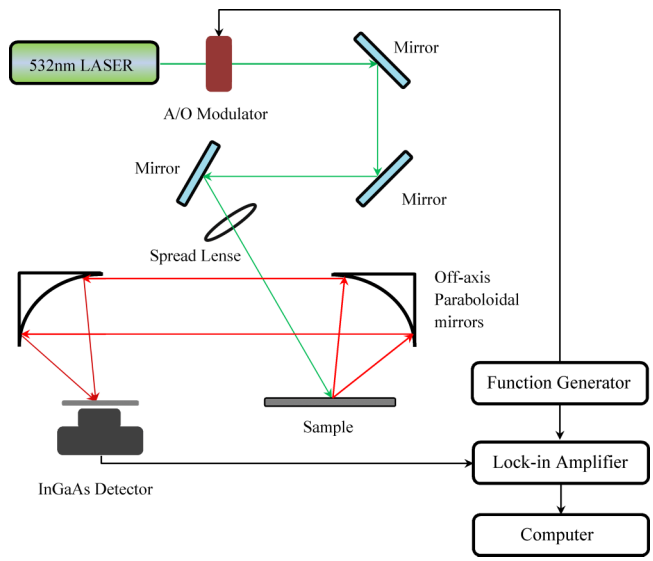

FIG. 3. Schematic diagram of the photocarrier radiometric setup.

TABLE I. Doping concentration in amorphous layer and thickness of i-a-Si.

Sample	Structure	Diborane-in-silane precursor gas concentration (%)	Thickness of i-a-Si (nm)
Wafer#1	(i-a-Si)/(n-c-Si)/(i-a-Si)	0	30
Wafer#2	(p-a-Si)/(n-c-Si)/(p-a-Si)	0.5	0
Wafer#3	(p-a-Si)/(n-c-Si)/(p-a-Si)	0.75	0
Wafer#4	(p-a-Si)/(n-c-Si)/(p-a-Si)	1.0	0
Wafer#5	(p-a-Si)/(i-a-Si)/(n-c-Si)/(i-a-Si)/(p-a-Si)	0.75	0
Wafer#6	(p-a-Si)/(i-a-Si)/(n-c-Si)/(i-a-Si)/(p-a-Si)	0.75	4
Wafer#7	(p-a-Si)/(i-a-Si)/(n-c-Si)/(i-a-Si)/(p-a-Si)	0.75	10

solver[8] to minimize the sum of the squares of errors between the experimental and calculated data starting with an initial estimate within a fixed interval. With this program, different starting points deliver different results and standard deviations (SDs) of the theoretical curve best-fitting to the experimental points. In order to investigate the reliability of the parameter measurements resulting from this solver, the procedure was repeated several hundred times and the 20 lowest variance results which lay below a pre-determined range interval were selected. In this manner, the mean value of each parameter and its SD, a measure of the scatter of the best-fitted results, were determined and for this reason measurements from this program were labeled "statistical best fits." The statistical mean value was used as reliability (uniqueness) measure and the SD as a precision measure of the associated parameter. The total duration of the multi-parameter fitting procedure does not exceed a few minutes.

III. INSTRUMENTATION AND MATERIALS

A schematic diagram of the experimental PCR system is shown in Fig. 3. A 532-nm laser (Coherent model Verdi V-10) was used in our experiments as a photocarrier excitation source. The 1.5-W beam was harmonically modulated using an acousto-optic modulator (ISOMET model 232-A) in the frequency range of 10 Hz to 100 kHz and was spread over a spot of 20-mm diameter on the sample surface. A long-pass filter (Spectrogon model LP-1000 nm) in front of the InGaAs detector prevented laser beam leakage onto the detector. Diffuse radiative-recombination-induced PCR signals were collected, collimated with two off-axis parabolodial mirrors, and focused onto the near-infrared InGaAs detector with spectral response in the 1.0-1.7 μm range. The detector signal was sent to a lock-in amplifier (Princeton Applied Research, model 5210) and the demodulated amplitude and phase were processed by a personal computer.

In order to investigate the influence of the doping concentration of the amorphous layer on the transport properties, 4 samples (wafers #1-4) were used as shown in Table I. Thin amorphous silicon films were deposited on silicon substrates using DC saddle field plasma enhanced chemical vapor deposition (DCSF-PECVD).[9] The thicknesses of i-a-Si and p-a-Si were all 30 nm and the thickness of the 1 Ω cm CZ n-c-Si substrate wafer was 290 μm for all samples in Table I.

Doping of the a-Si:H layer was controlled through the precursor gas composition: for p-type doping a diborane-silane gas mixture was used, with the diborane concentration, $[B_2H_6]/([B_2H_6]+[SiH_4])$, varied to achieve controlled changes in doping concentration.[9] The four samples were processed with diborane-in-silane precursor gas concentrations of 0, 0.5%, 0.75%, and 1%. In addition, wafers #5-7, Table I, were processed to test the effect of introducing an intrinsic amorphous layer in between the doped amorphous layer and the silicon substrate. The intrinsic layers which were

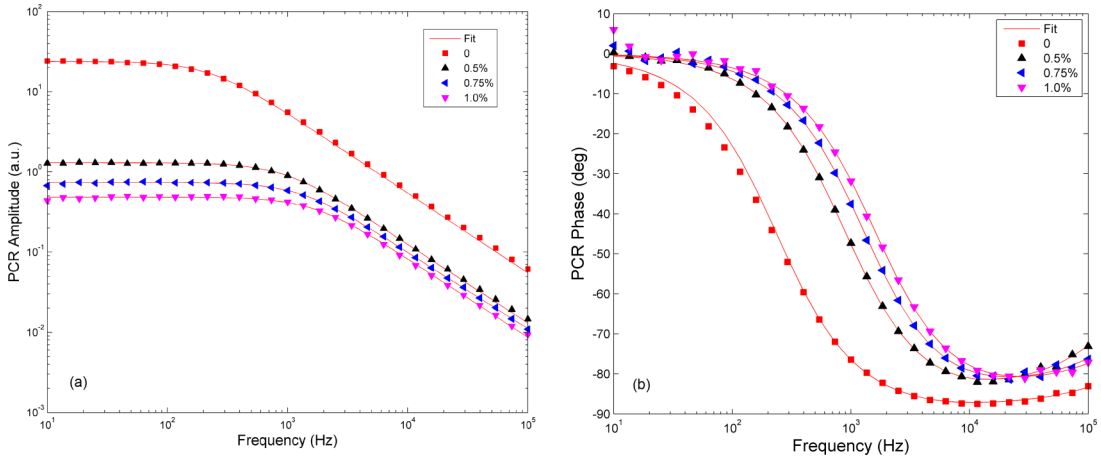

FIG. 4. PCR frequency scans of silicon wafers #1, #2, #3, and #4 with various doping concentrations in the a-Si layer (inset). (a) Amplitude and (b) phase.

deposited using only silane as a precursor gas were approximately 4 nm and 10 nm thick. The precursor gas dopant concentration corresponding to the amorphous silicon layers was 0.75%.

IV. RESULT AND DISCUSSION

A. Doping density dependent measurements

The PCR frequency scans of the four silicon wafers with various a-Si doping levels are shown in Fig. 4. It is observed that the PCR amplitude of the c-Si wafer with an undoped a-Si:H layer deposited on both sides is larger than that of all doped a-Si:H deposited wafers. As will be shown below (Table II), this work established that this effect is due to the lower front- and back-surface recombination velocities of the undoped sample. All the phases exhibit saturation at high frequencies followed by reversal, as the result of the trade-off between a trend for larger phase lag due to the finite recombination lifetime of photocarriers mostly in the substrate, and a counter-trend for smaller phase lag due to increased trapping rates at or near the nanolayer boundaries close to the surface. It is worth mentioning that on flipping the wafer over, essentially the same frequency dependencies were obtained, as expected from the symmetric geometry of the investigated samples (Table I).

Results of multi-parameter best-fits of the theoretical model to the data from wafers #1-4 are shown in Table II.

In the calculations, the absorption coefficient of the wafer substrate was assumed to be 7.85×10^5 m^{-1} which corresponds to crystalline silicon at 532-nm wavelength.[10] For simplicity, the absorption coefficients of the amorphous layer were all considered to be 1.49×10^7 m^{-1} regardless of doping density.[11] The carrier diffusion coefficient of the silicon wafer bulk was assumed to be 12 cm^2/s, corresponding to the calculated ambipolar diffusivity. It should be mentioned that for simplicity reasons, we used the 2-layer theory of Sec. II to fit the PCR data from all samples. This simplification is not crucial because the local recombination rate of diffusing photocarriers reaching the backside amorphous layer, which is only 30 nm thick, can be incorporated into an effective back surface recombination velocity. Similarly, the nm-thick i-a-Si:H layer was very thin compared to the CDW wavelength $\frac{1}{|\sigma_2|}$ even at the highest modulation frequency f = 100 kHz ($\sim\mu$m), which justified reducing the CDW solution at the interface to boundary conditions Eqs. (5) and (6). The best-fitted results show that the values from the mean-value best-fit computational program are all close to those obtained with the independent statistical best fit program. The interpretation of these consistent measurements is that the fitted results are considered reliable and thus the derived measurement values are statistically unique. It can be seen that the lifetimes τ_2 of the c-Si substrate in the four samples of Table II exhibit similar values, as expected from the same properties of the c-Si substrate. The front and back SRVs, S_1 and S_2, show increasing trends, Figs. 5(a) and 5(b), which are at least partly responsible for the large amplitude decreases with increasing doping concentration of the amorphous layer, Fig. 4.

TABLE II. Measured transport parameters of the front surface a-Si:H nanolayer and the substrate with various a-Si layer doping concentrations.

	Undoped a-Si		0.5% diborane-in-silane precursor gas concentration		0.75% diborane-in-silane precursor gas concentration		1% diborane-in-silane precursor gas concentration	
Fitted parameter	Mean-value best fit	Statistical fit	Mean-value best fit	Statistical fit	Mean-value best fit	Statistical fit	Mean-value best fit	Statistical fit
Recombination lifetime in c-Si wafer τ_2, s	1.31×10^{-3}	$1.38 \times 10^{-3} \pm 1.3 \times 10^{-4}$	1.07×10^{-3}	$1.16 \times 10^{-3} \pm 3.42 \times 10^{-4}$	1.12×10^{-3}	$1.31 \times 10^{-3} \pm 2.77 \times 10^{-4}$	1.13×10^{-3}	$1.12 \times 10^{-3} \pm 3.88 \times 10^{-4}$
Interface recombination velocity S_i, m/s	9.8×10^{-1}	$4.16 \times 10^{-1} \pm 2.36 \times 10^{-1}$	7.69×10^{-1}	$1.27 \pm 9.03 \times 10^{-1}$	3.29×10^{-1}	1.21 ± 1.48	1.48	$9.83 \times 10^{-1} \pm 8.31 \times 10^{-1}$
Front surface recombination velocity of a-Si:H layer S_1, m/s	1.02×10^{-1}	$1.49 \times 10^{-1} \pm 3.7 \times 10^{-2}$	1.69	2.69 ± 1.75	2.59	3.21 ± 1.83	2.96	3.58 ± 1.44
Effective back surface recombination velocity S_2, m/s	6.8×10^{-3}	$5.96 \times 10^{-3} \pm 7.9 \times 10^{-3}$	3.28×10^{-2}	$1.24 \times 10^{-1} \pm 1.24 \times 10^{-1}$	3.1×10^{-1}	$3.23 \times 10^{-1} \pm 1.46 \times 10^{-1}$	6.46×10^{-1}	$7.37 \times 10^{-1} \pm 1.28 \times 10^{-1}$
Diffusion coefficient in a-Si:H layer D_1, m^2/s	8.34×10^{-8}	$5.88 \times 10^{-8} \pm 1.74 \times 10^{-8}$	4.91×10^{-7}	$1.6 \times 10^{-7} \pm 1.07 \times 10^{-7}$	2.28×10^{-7}	$3.06 \times 10^{-7} \pm 2.47 \times 10^{-7}$	3.26×10^{-7}	$3.67 \times 10^{-7} \pm 2.78 \times 10^{-7}$
Recombination lifetime in i-a-Si:H layer τ_1, s	3.43×10^{-7}	$5.91 \times 10^{-7} \pm 2.39 \times 10^{-7}$	1.56×10^{-7}	$4.34 \times 10^{-7} \pm 2.96 \times 10^{-7}$	2.04×10^{-7}	$4.17 \times 10^{-7} \pm 2.96 \times 10^{-7}$	4.65×10^{-7}	$4.66 \times 10^{-7} \pm 2.65 \times 10^{-7}$
Density of free (unoccupied) traps at interface n_{Tf}, m^{-3}	3.18×10^{21}	$6.82 \times 10^{21} \pm 2.32 \times 10^{21}$	1.49×10^{21}	$1.48 \times 10^{21} \pm 6 \times 10^{20}$	1.49×10^{21}	$1.23 \times 10^{21} \pm 4.03 \times 10^{20}$	9.29×10^{20}	$1.23 \times 10^{21} \pm 4.28 \times 10^{20}$

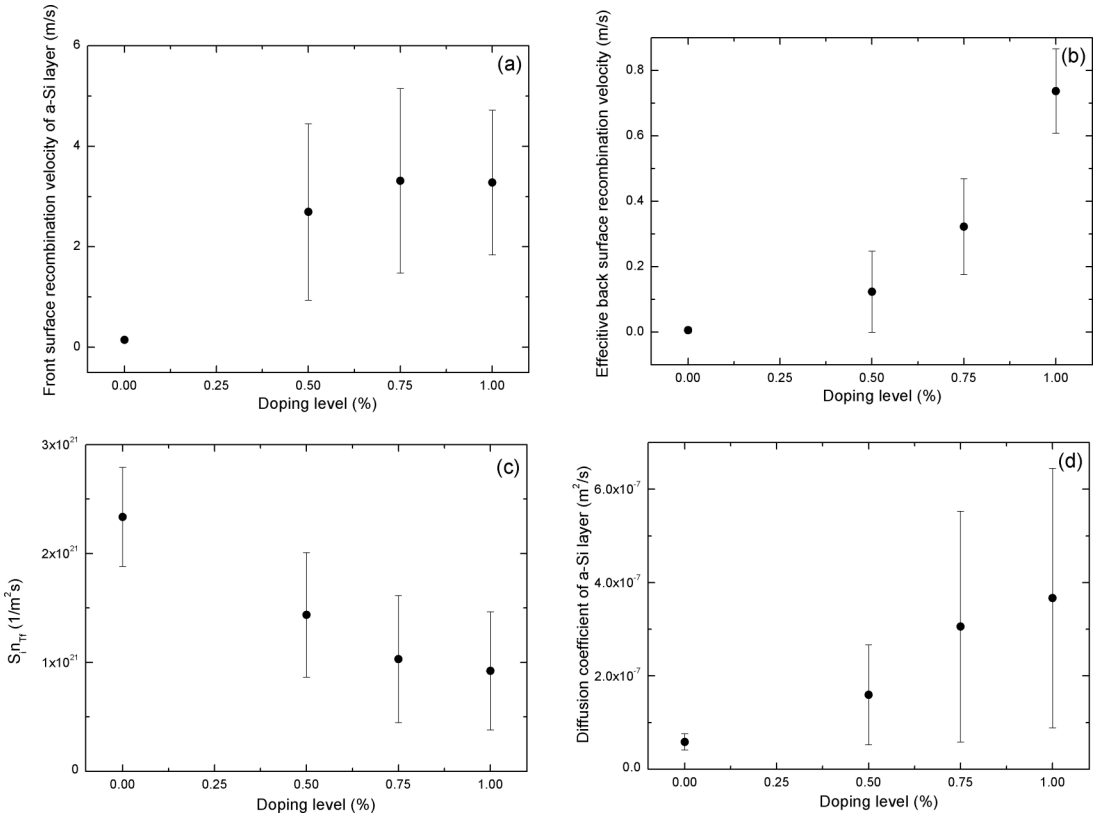

FIG. 5. Statistical best-fit computational program results with increasing precursor gas dopant concentration corresponding to the amorphous silicon layers. (a) Front SRV, (b) effective back SRV, (c) product of interface recombination velocity and free trap density (interface carrier density flux, F_i), and (d) diffusion coefficient of amorphous layer.

Comparing the mean values and the SDs of the back SRVs of the a-Si:H layer-deposited samples in the statistical best-fit program, it can been seen that they are of the same order of magnitude, which is interpreted as a measure of poorer measurement precision than other parameters. A similar conclusion can be made about S_i. Nevertheless, if the interface recombination velocity and the unoccupied trap density are grouped together as $F_i = S_i n_{Tf}$, a decreasing trend appears (a decreased interface carrier flux which controls the unoccupied trap density) with increasing doping density, Fig. 5(c). This is physically expected from the occupation (filling) of more traps at higher excess free carrier density generated from the increased doping density. The diffusion coefficient D_1 in the amorphous layer exhibits progressively larger SD with increasing a-Si doping density, Fig. 5(d), yet the mean value also increases. This trend can be understood in terms of an increased CDW diffusion length as a result of decreased unoccupied trap density with increasing doping density. This is also consistent with the measured free-trap decreasing density, fn_T, at the interface, Table II.

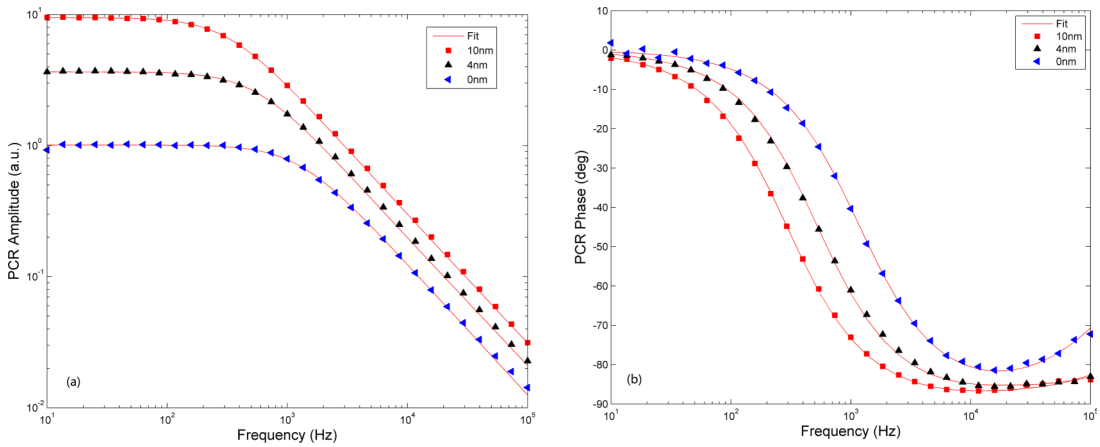

FIG. 6. PCR frequency scans of the Silicon wafers #5, #6, and #7 with various thicknesses of i-layer (inset). (a) Amplitude and (b) phase.

B. Intrinsic interface layer thickness dependent measurements

PCR frequency scans of Si wafers #5, #6, and #7 deposited with 0, 4, and 10 nm thickness of i-layer between the a-Si and c-Si layer, respectively, are shown in Fig. 6. The amplitude increases with increasing i-layer thickness due to passivation and reduction of recombination sites (decreased effective SRVs in the simplified two-layer model) at the front and back interfaces between the a-Si:H layer and the c-Si substrate. The intrinsic a-Si layers play very important roles, lowering defect densities at the interfaces between doped a-Si and c-Si layers. Without the intrinsic a-Si thin layers, recombination via defects in the doped a-Si would be significant to the detriment of performance of solar cells processed and fabricated with this thin-layer structure.

The best fitted parameters for substrate and upper layer with no i-layer and the two i-layer thicknesses are shown in Table III. Comparing the resulting parameters from the two independent best-fitting methods, the values from the mean-value best-fit are all within the range of those from the independent statistical best-fit calculation, an indicator that the thus measured parameters are statistically reliable and effectively unique within the standard deviations shown in Table III.

The i-a-Si:H layer thickness change from 0-10 nm between the a-Si and c-Si layers does not lead to any noticeable changes in substrate lifetimes, as physically expected. The front and back SRVs, S_1 and S_2, exhibit decreasing trends, Figs. 7(a) and 7(b), with increasing i-layer thickness.

However, the back SRV at the two non-zero i-a-Si thicknesses exhibits standard deviation larger than the mean value. This is not surprising as Fig. 7(b) clearly indicates that there is a large drop in this parameter to virtually zero level upon introduction of the i-a-Si interface layer. These results show that the effect of this layer is the decrease in the associated SRV value and is the single most significant factor in the large PCR amplitude increases with increasing layer thickness. The effect on the front SRV is similar to the back SRV as shown in Fig. 7(a). The product of the interface recombination velocity and the carrier density flux, $F_i = S_i n_{Tf}$, which controls the unoccupied trap density, Fig. 7(c), shows an increasing trend with increasing i-layer thickness. This trend is likely due to the increased effective number of unoccupied states within the i-layer. Increasing thickness enhances the interface F_i into these states; however, the traps no longer behave mainly like nonradiative decay centers as those which exist at the amorphous-layer substrate interface, but like intrinsic states close to the photoexcited front surface. As such, they can enhance radiative recombination pathways of the free CDW and contribute to the increase of the PCR amplitude. Consistent with this interpretation is the decrease in upturn of high-frequency PCR phase lag (>10 kHz) which exhibits saturation with minimal upturn at ~−90°, Fig. 6(b), approaching the case of the PCR response from a c-Si wafer without deposited surface layers.[12] Table III further shows that there are no clear trends in diffusion coefficient and lifetime of the a-Si:H layer. This is expected, as the physical recombination processes which determine the CDW diffusion length in

TABLE III. Measured transport parameters of the front surface a-Si:H nanolayer and the substrate with various i-layer thicknesses between the a-Si layer and the substrate.

	i-a-Si thickness (nm)					
	0		4		10	
Fitted parameter	Mean-value best fit	Statistical fit	Mean-value best fit	Statistical fit	Mean-value best fit	Statistical fit
Recombination lifetime in c-Si wafer τ_2, s	1.09×10^{-3}	$1.10 \times 10^{-3} \pm 3.59 \times 10^{-4}$	1.28×10^{-3}	$1.07 \times 10^{-3} \pm 3.82 \times 10^{-4}$	1.13×10^{-3}	$1.29 \times 10^{-3} \pm 2.06 \times 10^{-4}$
Interface recombination velocity S_i, m/s	1.99	1.06 ± 1.09	3.49×10^{-1}	$5.25 \times 10^{-1} \pm 3.38 \times 10^{-1}$	7.5×10^{-1}	$8.07 \times 10^{-1} \pm 4.5 \times 10^{-1}$
Front surface recombination velocity of a-Si:H layer S_1, m/s	2.78	3.48 ± 2.99	7.09×10^{-1}	$5.97 \times 10^{-1} \pm 1.93 \times 10^{-1}$	1.7×10^{-1}	$2.84 \times 10^{-1} \pm 8.3 \times 10^{-2}$
Effective back surface recombination velocity S_2, m/s	2.79×10^{-1}	$5.05 \times 10^{-1} \pm 1.83 \times 10^{-1}$	4.91×10^{-2}	$9.15 \times 10^{-3} \pm 1.99 \times 10^{-2}$	9.06×10^{-3}	$8.89 \times 10^{-3} \pm 1.11 \times 10^{-2}$
Diffusion coefficient in a-Si:H layer D_1, m^2/s	1.49×10^{-7}	$2.01 \times 10^{-7} \pm 1.72 \times 10^{-7}$	6.9×10^{-7}	$4.44 \times 10^{-7} \pm 3.1 \times 10^{-7}$	5.98×10^{-8}	$9.65 \times 10^{-8} \pm 5.68 \times 10^{-8}$
Recombination lifetime in i-a-Si:H layer τ_1, s	4.78×10^{-7}	$4.29 \times 10^{-7} \pm 3.04 \times 10^{-7}$	5.92×10^{-7}	$3.74 \times 10^{-7} \pm 2.95 \times 10^{-7}$	5.04×10^{-7}	$5.68 \times 10^{-7} \pm 3.04 \times 10^{-7}$
Density of free (unoccupied) traps at interface n_{Tf}, m^{-3}	9.12×10^{20}	$1.6 \times 10^{21} \pm 5.96 \times 10^{20}$	3.42×10^{21}	$3.43 \times 10^{21} \pm 1.31 \times 10^{21}$	3.81×10^{21}	$3.71 \times 10^{21} \pm 1.46 \times 10^{21}$

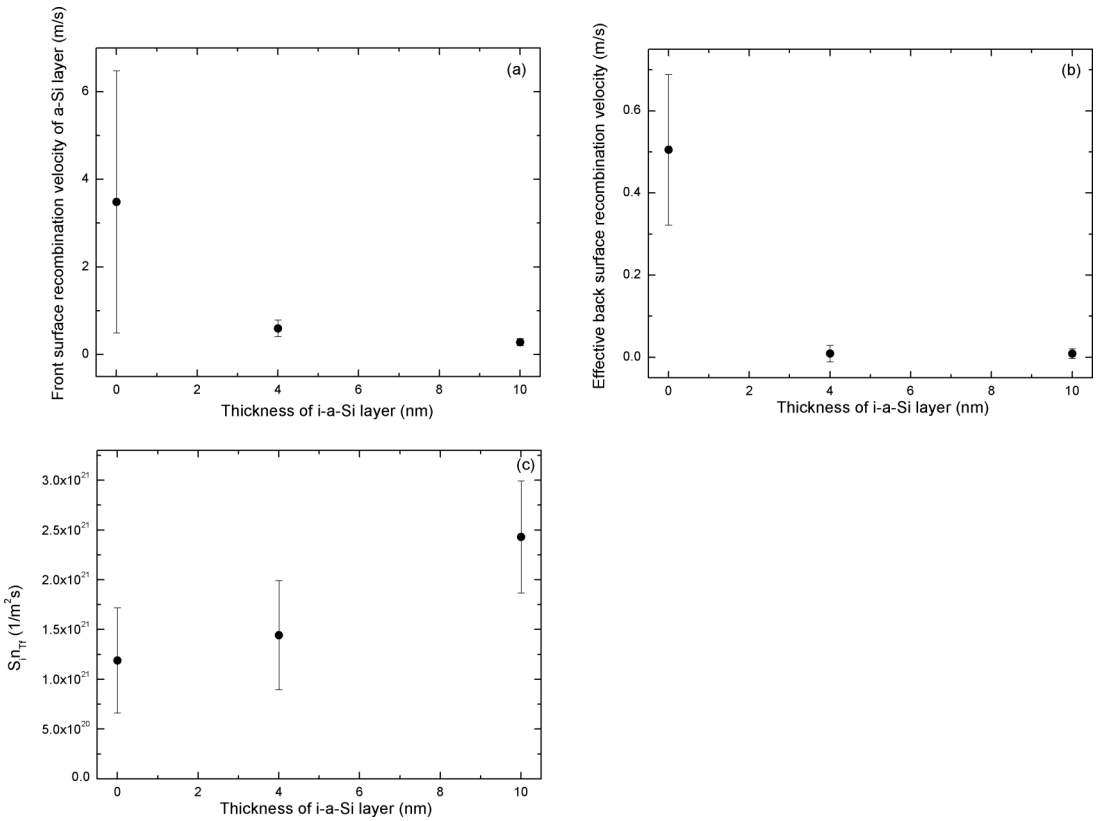

FIG. 7. Statistical best-fit computational program results with increasing i-layer thickness. (a) Front surface recombination velocity, (b) effective back surface recombination velocity, and (c) product of interface recombination velocity and free trap density (interface carrier density flux, F_i).

a-Si:H remain unchanged with changing interface i-a-Si layer thickness.

V. CONCLUSIONS

Photocarrier radiometry with modulated 532-nm laser excitation showed excellent sensitivity for the characterization of optoelectronic transport processes in hydrogenated doped amorphous/crystalline silicon heterojunctions with a buffer i-a-Si:H layer used for solar cell fabrication. A 1-D two-layer PCR theoretical model was developed for the quantitative evaluation of the effects of a-Si doping concentration and buffer i-a-Si:H layer thickness on the transport properties of the heterojunction structure. This allowed the study of reliability of multi-parameter best fits to data with only two signal channels (amplitude and phase) through two independent best-fit computational programs, a "mean-value best fit" and a "statistical best fit." Both computational programs yielded seven parameter value sets (carrier recombination lifetimes, diffusion coefficients, front- and back-surface and interface recombination velocities, as well as effective unoccupied trap densities at the interface) in the same range, thereby empirically establishing the statistical uniqueness of the parameter measurements. The size of the standard deviations obtained with the statistical best fit was used as a criterion for measurement precision of all the parameters. These quantitative results showed that increasing the doping concentration of the amorphous silicon layer leads to increases in the front- and back-surface recombination velocities. They also showed that increasing the thickness of the buffer i-a-Si:H between the amorphous layer and the c-Si layer leads to decreases in the effective front- and back-surface recombination velocities.

ACKNOWLEDGMENTS

The authors are grateful to the Natural Sciences and Engineering Research Council of Canada (NSERC) for a Discovery Grant to A. Mandelis, to the Canada Foundation for Innovation (CFI) for equipment grants, and to the Canada Research Chairs Program.

[1]M. Taguchi, A. Yano, S. Tohoda, K. Matsuyama, Y. Nakamura, T. Nishiwaki, K. Fujita, and E. Maruyama, "24.7% record efficiency HIT solar cell on thin silicon wafer," IEEE J. Photovoltaics **4**, 96-99 (2014).
[2]http://news.panasonic.com/press/news/official.data/data.dir/2014/04/en140410-4/en140410-4.html.
[3]L. Korte and M. Schmidt, "Investigation of gap states in phosphorous-doped ultra-thin a-Si:H by near-UV photoelectron spectroscopy," J. Non-Cryst. Solids **354**, 2138-2143 (2008).
[4]L. Korte, E. Conrad, H. Angermann, R. Stangl, and M. Schmidt, "Advances in a-Si:H/c-Si heterojunction solar cell fabrication and characterization," Sol. Energy Mater. Sol. Cells **93**, 905 (2009).
[5]S. M. de Nicolás, D. Muñoz, A. S. Ozanne, N. Nguyen, and P. J. Ribeyron, "Optimisation of doped amorphous silicon layers applied to heterojunction solar cells," Energy Procedia **8**, 226-231 (2011).
[6]B. Li, D. Shaughnessy, and A. Mandelis, "Mesurements accuracy analysis of photocarrier radiometric determination of electronic transport properties of silicon wafers," J. Appl. Phys. **97**(2), 023701 (2005).

[7]A. Melnikov, A. Mandelis, B. Halliop, and N. P. Kherani, "Effective interface state effects in hydrogenated amorphous-crystalline silicon heterostructures using ultraviolet laser photocarrier radiometry," J. Appl. Phys. **114**(24), 244506 (2013).
[8]J. D'Errico, http://www.mathworks.com/matlabcentral/fileexchange/8277.
[9]B. Halliop, M. F. Salaun, W. Favre, R. Varache, M. E. Gueunier-Farret, J. P. Kleider, and N. P. Kherani, "Interface properties of amorphous-crystalline silicon heterojunctions prepared using DC saddle-field PECVD," J. Non-Cryst. Solids **358**(17), 2227-2231 (2012).
[10]E. D. Palik, *Handbook of Optical Constants of Solids* (Academic, San Diego, 1998).
[11]M. A. Green, "Self-consistent optical parameters of intrinsic silicon at 300 K including temperature coefficients," Sol. Energy Mater. Sol. Cells **92**(11), 1305-1310 (2008).
[12]A. Mandelis, *Diffusion-Wave Fields* (Springer, New York, 2001), Chap.9.